Acta Crystallographica Section A
Foundations of Crystallography
ISSN 0108-7673

Received 13 August 2004
Accepted 12 November 2004

The structure of short-lived excited states of molecular complexes by time-resolved X-ray diffraction

Philip Coppens,[a]* Ivan I. Vorontsov,[a] Tim Graber,[b] Milan Gembicky[a] and Andrey Yu. Kovalevsky[a]

[a]Department of Chemistry, State University of New York at Buffalo, NY 14260, USA, and [b]University of Chicago, IL 60637, USA. Correspondence e-mail: coppens@acsu.buffalo.edu

Experimental and computational methods for time-resolved (TR) diffraction now allow the determination of geometry changes on molecular excitation. The first results indicate significant changes in the interatomic distances and molecular shape on photo-excitation, but also a dependence of the induced changes on the molecular environment. Though the use of high-brightness synchrotron sources is essential, it limits the time resolution to the width of the synchrotron pulse which is currently 70–100 ps. The experiments discussed fall into two categories: (i) picosecond powder diffraction experiments on the molecular excitation to a singlet state, and (ii) microsecond experiments on the excited states of inorganic complexes. Both involve reversible processes for which a stroboscopic technique can be applied.

© 2005 International Union of Crystallography
Printed in Great Britain – all rights reserved

1. Introduction

During the decades since the 1912 discovery of X-ray diffraction with the dramatic experiments of von Laue and co-workers, X-ray crystallography has developed into the prime technique for determination of small and large molecular structures. Though its capabilities are now taken for granted by the scientific community, it is well documented that reaching this level of accomplishment required the efforts of many outstanding scientists.

Though the X-ray scattering process is very fast ($\sim 10^{-18}$ s), data collection is much slower, so that the resulting image corresponds to a time (and space) average over the diffracting crystal. This situation is now changing. With the increasing intensity and brightness of the now available sources, ever smaller objects can be imaged and diffraction patterns can be measured on ever shorter time scales, so that the averaging is over a shorter and shorter time interval. This fundamental advance is opening up the field of time-resolved diffraction, thereby generalizing X-ray crystallography into a fourth (time) dimension, and extending the field into an area of great importance in the natural sciences, including chemistry and biology in which many processes proceed extremely rapidly.

The techniques used in time-resolved (TR) biochemical crystallography and in chemistry–materials-science applications differ in that in the former the polychromatic Laue technique is combined with a low-repeat-rate laser, while in the latter monochromatic techniques are commonly employed, often in conjunction with fast-repeat-rate lasers. However, the techniques are converging as discussed further below.

An important distinction is between reversible and irreversible processes, where the word reversible implies that the system reverts to the initial state after a certain time span, even though the excitation process is not reversible at any point along its path. Fully reversible processes can be initiated repeatedly at very high repeat rates and examined stroboscopically, while irreversible processes can be studied only once with a given crystalline sample.[1]

A second classification is between experiments that aim at establishing the structure of a transient species and those aimed at following a dynamic process with time. For the latter, the pump-probe delay may be varied in a series of experiments (Schotte *et al.*, 2003; Anderson *et al.*, 2004), and the challenge is to produce a 'movie' (Ren *et al.*, 2001; Srajer *et al.*, 2001), tracking the progress of the dynamic change at the atomic level as it proceeds. Because of the much less efficient use of the X-ray beam when the synchrotron time structure is used (see below), as necessary for the monitoring of fast processes, the latter has so far only been achieved with protein-Laue or powder techniques (Techert *et al.*, 2001; Moffat, 2001; Techert & Zachariasen, 2004). This classification of TR studies is summarized in Table 1.

When single-crystal methods are used, the requirement that crystal integrity be preserved as the reaction proceeds poses a limitation. But it has been shown that reactions such as the dimerization of cinnamic acid and its derivatives can be made to proceed without the loss of crystallinity (Enkelmann *et al.*,

[1] In a recent macromolecular experiment, it has been possible to irradiate different parts of a crystallite in subsequent exposures (Schotte *et al.*, 2003), but this technique may not be applicable in high-resolution experiments.

Table 1
Classification of time-resolved experiments.

	Reversible processes	Irreversible processes
Structure of transient species	Equilibrated excited states	Reactive intermediates
'Molecular movie'	Non-equilibrated excited states	Chemical reaction paths

1993), whereas the field of crystal engineering offers the possibility of performing reactions in the less constraining environment of the channels and cavities in a supramolecular framework. In protein crystallography, in which very large molecular entities are positioned in a solvent environment, the danger of crystal breakdown as a result of the light-induced process is much less severe or absent, prime examples being several studies on the dissociation and recombination of CO in myoglobin and the photoreaction in photoactive yellow protein (Schotte *et al.*, 2002, 2003; Rajagopal *et al.*, 2004; Anderson *et al.*, 2004).

It should be emphasized that the remainder of this manuscript deals exclusively with time-resolved studies of excited-state structure in solids and not with the field of macromolecular time-resolved diffraction. The pioneering picosecond timescale studies of the cooperative phase transition in tetrathiafulvalene-*p*-chloranil of Collet *et al.* (2003) and Guérin *et al.* (2004) are also beyond the scope of this article. §2 on technical aspects specifically deals with atomic resolution single-crystal methods. However, in §4, the results of ps-timescale powder diffraction studies of the singlet excited state of amino-substituted benzonitriles, performed at ESRF, are included.

2. Technical aspects

2.1. The use of pump-probe techniques

A crucial part of the time-resolved experiment is the initial triggering of the dynamic process. If the trigger is too slow, time resolution is correspondingly limited. In slower TR studies, triggers such as temperature jumps (as in solid-state reactions) (Wong *et al.*, 1990; Rodriguez *et al.*, 2002) and fast mixing (the latter only applicable to solutions of course) are used, but these are not suited for the μs and sub-μs experiments that are needed to study short-lived species and fast reactions. Thus, lasers are widely used to initiate the processes to be studied. They include photochemical reactions, photoexcitation (often as the first step in a photochemical reaction) and photo-induced phase transitions. In such experiments, the laser pulse is the *pump* pulse, which is synchronized with the following X-ray *probe* pulse. If a rapid irreversible process is to be studied, only a single pulse can be used in each experiment, but the delay time can be varied to map the geometry change along the reaction path in a series of consecutive experiments. With currently available sources, the intensity limitations imposed by the use of a single pulse dictates the use of powder diffraction methods or polychromatic Laue techniques. For reversible processes in more robust crystals, a stroboscopic experiment can be performed that greatly reduces the intensity limitations. With this technique, a large number of reflections can be collected and quasi-conventional crystallographic structure analysis techniques can be used.

2.1.1. The stroboscopic pump-probe technique. In the stroboscopic pump-probe experiment, the crystal is repeatedly excited and probed following excitation, after which it is allowed to relax before the next pump-probe cycle. The experiment can be performed at high repeat rates, thus allowing accumulation of a number of counts for each reflection commensurate with statistical requirements, even when narrow-energy-bandwidth monochromatic radiation is used. The laser repeat rates are limited by the following requirements.

(i) Each laser pulse contains a number of photons of the same order of magnitude as the number of photoactive molecules in the crystal, which is of the order of 10^{13}–10^{15} for a typical crystal with 40–80 μm linear dimension. As the power per pulse is a function of the laser repeat rate (see below), this introduces a limitation. To ensure uniformity of illumination over the volume of the sample crystal, absorption of the light in the sample must be limited to ~10%. An equally compelling reason to avoid very high transient conversion is that the resulting increased release of energy increases the likelihood of rapid breakdown of the crystal.

(ii) Heat be dissipated as rapidly as possible to preserve the crystal's integrity under rapidly repeating laser pulses.

(iii) Crystal quality is preserved for a time long enough to collect a substantial number of reflections.

These considerations make it necessary to use small crystals, which must be enveloped by a cryogenic, preferably helium, gas flow. It may be noted that in some cases cryocooling could interfere with the conformational changes to be studied, which would prevent the use of powerful high-repeat-rate lasers.

Laser technology is developing rapidly and is continuously being improved. The Nd vanadate laser used at APS has a fundamental frequency of 1064 nm and, equipped with a frequency doubler or tripler, produces light at 532 and 355 nm, respectively. Its total power, pulse width and their dependence on the repetition rate are illustrated in Fig. 1 for 355 nm light. The power peaks at about 20 kHz and decreases when the repeat frequency is increased further. At 532 nm, the output is about 2.5 times larger. The time resolution that can be achieved with these lasers is limited by their 30–50 ns pulse widths, which exceeds the ~100 ps synchrotron pulse width. The latter constitutes an intrinsic lower limit to the time resolution until narrower-pulse-width sources with high brightness become available. For shorter timescales than accessible with the Nd vanadate laser, a more complex Ti:sapphire laser with ~100 fs pulse width can be used (Wulff *et al.*, 2003). However, such lasers cannot operate at repeat rates much higher than 1 kHz and at the same time produce sufficient power per pulse, and they need auxiliary lasers for pumping and amplification. A recently announced diode-pumped Yb tungstate laser with a 500 fs pulse width is much

simpler to operate, has higher average power than Ti:sapphire lasers, and a repeat rate up to 7 kHz (Krueger & Féru, 2004).

The 100 fs pulse-width Ti:sapphire laser was used in the fast powder diffraction experiments at ESRF, with a tripler to produce a wavelength of 267 nm and 5–8 μJ per pulse (Techert & Zachariasen, 2004). In this experiment, the frequency of 897 Hz was imposed by the need to use a subharmonic of the orbit frequency of the storage ring, and mechanical limitations of the triangular shutter used (Wulff *et al.*, 2003).

2.1.2. Strategy for stroboscopic single-crystal data collection. The strategy developed for the single-crystal stroboscopic data collection is schematically illustrated in Fig. 2 (Fullagar *et al.*, 2000). A frame of data is collected while the crystal is rotated over a narrow range (typically 0.3°) under exposure to the laser pulses. The same frame is then collected under laser-off conditions.

The laser-on and laser-off measurements follow each other with a separation of only the time needed for detector readout, thus allowing an essentially *differential* measurement. The minimal delay between on and off measurements ensures that long-range fluctuations in the intensity of the beam hitting the crystal and, importantly, early deterioration of crystal quality in the intense laser beam are eliminated in the calculation of intensity differences, leading to a much more sensitive probe of the often small intensity changes that occur on excitation of the part of the molecules in the crystal.

The on–off sequence is repeated for additional frames until data collection is complete or crystal quality deteriorates due to the prolonged laser exposure.

A schematic of the set-up in use at the 15-ID station at the Advanced Photon Source at Argonne National Laboratory is shown in Fig. 3. The luminescence and diode detectors are used for the control of the pump–probe synchronization. The chopper wheel shown is described in the following section.

The experimental procedure for time-resolved powder data collection is much simpler as the need for stepwise frame collection in the single-crystal experiment is eliminated. However, for all experiments, the pump–probe synchronization has to be increasingly accurate as the time resolution increases.

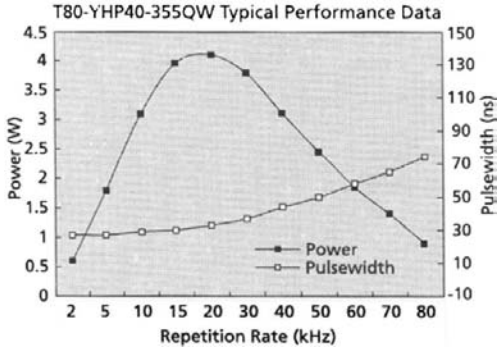

Figure 1
Time-averaged laser power and pulse width for the pulsed SpectraPhysics Nd vanadate laser in use at APS 15-ID at 355 nm.

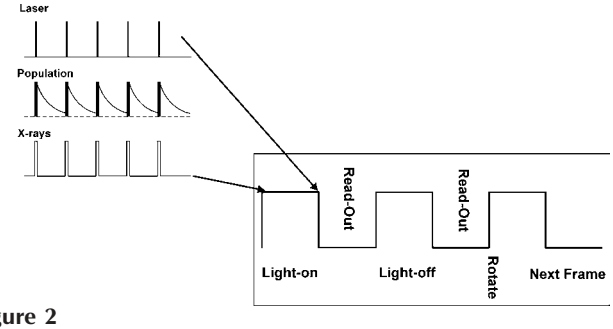

Figure 2
Time structure and data-collection strategy of the stroboscopic diffraction experiment. The diagram at the top left illustrates the temporal structure of the pump–probe procedure. The pump/probe pulses are repeated 5000–25000 times per second in the stroboscopic single-crystal experiments described below. The X-ray probe pulse can be delayed relative to the pump pulse, which may be desirable if, for example, a long-lived excited state is to be studied after a shorter lifetime state has fully decayed.

2.2. The X-ray duty cycle and the distinction between μs and sub-μs experiments

When the synchrotron beam is treated as a continuous source, pulses can be generated with a rapidly rotating chopper wheel with narrow slots at equidistant intervals (Fig. 4). This approach leads to more efficient use of the beam for a time resolution down to about the orbit time of the synchrotron (2.82 μs at ESRF, 3.68 μs at APS, 4.78 μs at SPring-8). For shorter time scales, the X-ray beam can no longer be treated as continuous. As mechanical shutters have speed limits and slot-size limitations, use of the time structure of the synchrotron beam with a non-uniform filling of the ring becomes imperative. We will treat the two approaches separately.

2.2.1. Use of the synchrotron as a continuous source. If R is the rotation speed of the wheel in rev min^{-1} and N the number of slots, the repeat frequency of the pulses in Hertz (*i.e.* per second) will be given by

$$\nu_P = NR/60$$

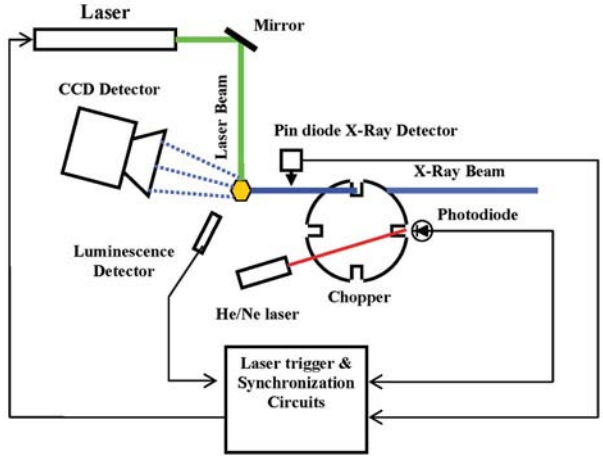

Figure 3
Schematic diagram of the time-resolved diffraction station at the 15-ID undulator beamline at the Advanced Photon Source.

while the time between pulses equals

$$T = 1/\nu_P = 60/(NR)\,\mathrm{s}$$

and the length of the X-ray pulse becomes

$$t_x = w/(\pi\oslash) \times 60/R$$

in which w is the slot width and $\oslash$ the effective diameter of the chopper wheel.

The duty cycle D, *i.e.* the fraction of the time the X-ray beam is utilized, becomes

$$D = Nw/(\pi\oslash) = t_x/T.$$

As a practical example, for a wheel with 240 slots of 300 μm width and an effective diameter of 135 mm, the duty cycle D is 17% and independent of the rotation speed. When this wheel is rotated at 4000 rev min^{-1}, the frequency of the X-ray pulses ν_p (which is to be matched by the frequency of the laser pulses) will be 16000 Hz, and the opening time 10.6 μs. In order to maximize the excited-state population in the experiment, the opening time should be less than the lifetime of the excited species, as illustrated in Fig. 5.

2.2.2. Using the time structure of the synchrotron source. The frequency of rotation of the electron bunches around the synchrotron is larger by a factor of ten or more than the repeat rate of a laser with suitable power per pulse. One of the functions of the X-ray shutter is therefore to reduce the repeat rate of the X-ray pulses to that of the laser. At the Advanced Photon Source, the flight time around the ring is 3.68 μs, corresponding to a single-bunch repeat rate of ~272 kHz. The shutter must reduce this rate to the 1–25 kHz range typically used in TR experiments and select the desired electron bunches from the bunch structure around the ring. Several types have been described, including shutters with a rotating disc (LeGrand *et al.*, 1989), a rotating cylinder (McPherson *et al.*, 2000) and a triangular rotor (Wulff *et al.*, 2003). To match the synchrotron time structure, both the rotation speed of the motor and the position of each opening must be extremely accurate in such an instrument.

During normal operation, the synchrotron pulses are quite closely spaced, for instance at APS in the normal 24 bunch top-up operating mode they are separated by only 153 ns. Since existing shutters cannot select single pulses when the separation is this small, the experiments must be performed during special operating modes (SOM) in which groups of pulses are more tightly spaced (the minimum is 2.84 ns) but separated from the other pulse(s). The special operating modes vary among the facilities and often can be changed with need. At APS, the following modes are currently among those that can be requested.

- SOM1. A single bunch, containing a maximum of 5 mA current, isolated from the remaining bunches by symmetrical 1.59 μs gaps, with the remaining current distributed in eight groups with a spacing of 48 ns between the groups, each with seven consecutive bunches at 2.84 ns spacing with a maximum current of 12 mA per group.
- SOM3. Three consecutive bunches with a maximum of ~15 mA current, isolated from the remaining bunches by symmetrical 1.59 μs gaps, with the remaining current distributed in eight groups of seven consecutive bunches with a maximum current of ~11 mA per group and a spacing of 48 ns between groups.

Selection of the single bunch of SOM1 gives the optimal time resolution corresponding to the width of a single pulse (100 ps at APS) but at the expense of a very small duty cycle. For a total ring current of 101 mA and a 5 mA single pulse,

$$D = (5/101)(\nu_{\mathrm{laser}}/\nu_{\mathrm{ring}}),$$

which gives duty cycles of only 0.45 and 0.18% for laser frequencies of 25 and 10 kHz, respectively!

If the remaining bunches of SOM1 (collectively referred to as a superbunch) are selected, the duty cycle is more favorable and close to $\nu_{\mathrm{laser}}/\nu_{\mathrm{ring}}$, as most of the current in the ring is utilized. But the time resolution will deteriorate to (for SOM1 at APS) $7 \times 48 + 8 \times 7 \times 2.84$ ns = 495 ns.

Similar considerations apply to SOM3. It is clear that the utilization of the X-ray flux, as expressed by the duty cycle D, deteriorates rapidly when a time resolution of better than a few hundred nanoseconds is needed. This decrease can be at least partly compensated for by modifying the optics such that a wider band pass of radiation is used.

2.3. The choice of X-ray band width

For the continuous-source experiments with a resolution of μs and for the pulsed-source experiments down to several hundred ns, monochromatic radiation from a silicon mono-

Figure 4
Mechanical chopper wheels for use in time-resolved single-crystal experiments.

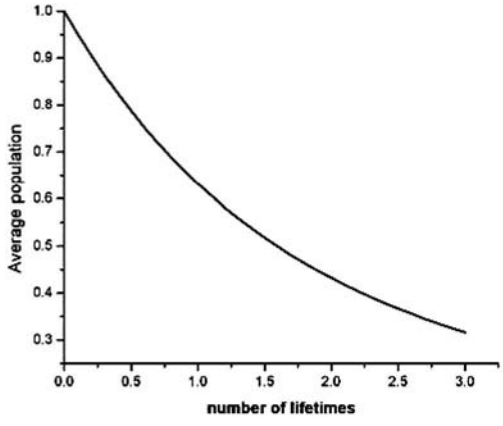

Figure 5
Excited-state population averaged over the X-ray exposure time per pulse *versus* X-ray pulse width in number of lifetimes following the laser pulse (the population is normalized to 1 at $t = 0$).

chromator with its advantages of narrow diffraction peaks is often adequate.

For faster experiments, the much lower value of the duty cycle requires more intensity than available with monochromatic radiation if atomic resolution is to be achieved by collection of large numbers of sufficiently strong single-crystal reflections, thus dictating the use of a broader band pass of wavelengths, with the concomitant increase in X-ray flux.

An excellent discussion of the advantages and disadvantages of the use of Laue techniques, especially at 'single-line' undulators with a band pass of a few keV, is given by Bourgeois *et al.* (2000). Wulff *et al.* (2003) report an increase by a factor of 460 compared with an Si(111) monochromator ($\Delta E/E \sim 10^{-4}$) when the first harmonic of the undulator at the U20 beamline at ESRF with $\Delta E/E$ of 2.37% is used. However, the undulator spectral distribution has a tail, which may be as long as 20% of $\Delta E/E$, and will affect the peak profile quality. This may lead to overlap of closely spaced reflections. An attractive alternative is the use of *multilayer* monochromators, consisting of alternating layers of a high- and a low-electron-density material, which are becoming increasingly available (Ziegler *et al.*, 2001; Headrick *et al.*, 2002; Martynov *et al.*, 2003). They can achieve $\Delta E/E$ values of ~1% depending on the number of layers in the monochromator and produce a 20–40 times increase in flux compared with a monochromatic beam. To counteract the decrease in duty cycle with increasing time resolution, use of such 'pink' beam techniques is essential in ultrafast TR single-crystal studies at atomic resolution.

3. Computational aspects

3.1. Real-time analysis of the intensity data

As synchrotron beamtime is a scarce commodity that must be optimally used, the induced intensity changes must be monitored in real time during data collection. A second diagnostic test involves internal agreement factors among the equivalent response ratios, defined as the fractional intensity changes, much like the merging R factor of conventional data collection.

Only part of the laser energy absorbed by the crystal is dissipated by light emission, the remainder being converted to heat through non-radiative processes. Although little information is available on the heat transfer to the cryogenic gas stream, our preliminary test experiments show that, under the experimental conditions employed at 15-ID at APS, even in the He stream the temperature increase persists for at least a hundred μs. The temperature increase is evident in a Wilson-type plot of $\ln(I_{on}/I_{off})$ *versus* $(\sin\theta/\lambda)^2$, which has a slope of $2\Delta B$, ΔB being the increase in the overall displacement parameter (Fig. 6). Part of this increase reflects the presence of the photo-induced static transient disorder in the crystal. Analysis of a simulated data set, mimicking the experimental results on $Cu^{I}(dmp)(dppe)PF_6$ (described below), indicates that in this experiment about 20% of the slope is due to the transient disorder (Vorontsov & Coppens, 2005).

Temperature increases are also evident from cell dimension changes. They are estimated to be between 10 and 40 K, depending on the details of the experiment.

When more than one data set has been collected, the consistency of the measurements can be examined by plotting the two sets of response ratios against each other. An example is shown in Fig. 7. An intensity increase is observed for a number of low-order reflections, but for the high-order reflections the temperature effect dominates, though they will still contain the signal of the geometry change.

3.2. Refinement of the structural changes

With the assumption of a random distribution of the excited-state molecules in the crystal, the structure-factor expression for elastic scattering is given by (Coppens, 1992; van Reeuwijk *et al.*, 2000)

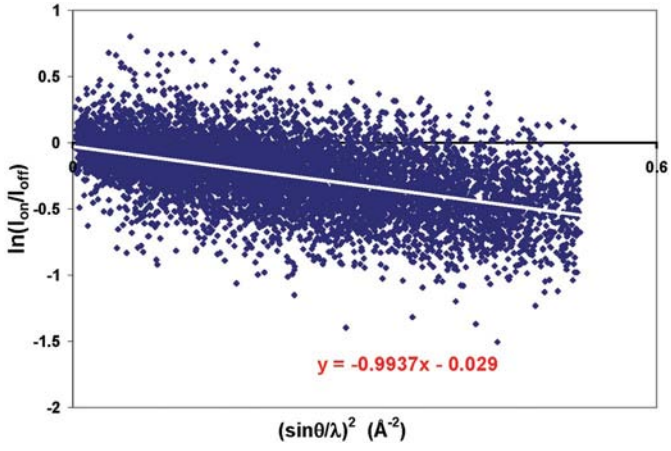

Figure 6
Wilson-type plot of $\ln(I_{on}/I_{off})$ *versus* $(\sin\theta/\lambda)^2$ for a data set of $[Cu^{I}(dmp)(dppe)]PF_6$.

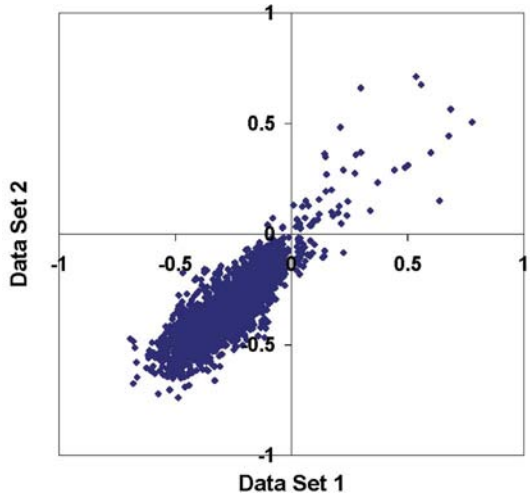

Figure 7
Correlation between two sets of response ratios for $[Rh_2(dimen)_4](PF_6)_2$ (1σ cutoff).

$$F_{on}(hkl) = (1 - P)F_{on,ground}(hkl) + PF_{on,excited}(hkl), \quad (1)$$

in which P is the excited-state population, and $F_{on,ground}(hkl)$ and $F_{on,excited}(hkl)$ are the structure factors for the ground- and excited-state species in the exposed crystal, respectively. The validity of the formalism in the case of photoinduced molecular excitation is supported by the absence of extra diffraction spots, which would indicate formation of domains with different cell dimensions and/or symmetry. Even for crystals with photoinduced metastable states of transition-metal nitrosyl compounds, with much higher conversion percentages than achieved in the time-resolved excited-state work (Carducci *et al.*, 1997; Coppens *et al.*, 1998, 2002; Kovalevsky *et al.*, 2002, 2003), no additional diffraction maxima were observed and expression (1) was successfully applied.

On the other hand, in the case of the photoinduced phase transition described by Collet *et al.* (2003), a cooperative transformation occurs with high quantum yield, and domain formation is evident. This invalidates the structure-factor formalism (1), instead

$$F_2(hkl) = (1 - x)F^2_{stable}(hkl) + xF^2_{photoinduced}(hkl) \quad (2)$$

must be used, where x is the volume fraction of the conversion, assuming that the change in cell dimensions is so small that corresponding spots overlap.

Since the experiment is designed to measure intensity changes, the least-squares minimization procedure is based on the *response ratios* $\eta(hkl)$, defined as the relative change in the intensities of the Bragg reflections under the external perturbation (Coppens, 1992; Ozawa *et al.*, 1998):

$$\eta(hkl) = \frac{I_{on}(hkl) - I_{off}(hkl)}{I_{off}(hkl)} = \frac{F^2_{on}(hkl) - F^2_{off}(hkl)}{F^2_{off}(hkl)}. \quad (3)$$

The least-squares refinement program *Laser04* (Vorontsov & Coppens, 2005), which is a considerably expanded variant of earlier software (Ozawa *et al.*, 1998), allows refinement of the temperature scale factor k_B (Ozawa *et al.*, 1998), the excited-state populations of each of the data sets included in the refinement, which may differ for independent molecules in the asymmetric unit, of positional parameters and of the position and orientation of rigid-body fragments of both the ground- and excited-state species. The rigid-body option becomes essential when large complexes are studied, as in one of the studies described below.

4. Overview of experimental results

The studies reported so far on excited-state geometry can be separated into two groups (here labeled A and B). The work by Techert *et al.* (2001) concerns fluorescent excited states with ps to ns lifetimes, in which attention was focused on the orientation of a substituent in the central six-membered ring of the compound to address a long-standing issue about the geometry of the intramolecular charge-transfer state of amino-substituted benzonitriles. The powder work involves analysis of a small number of reflections in a series of patterns collected at 50 ps intervals.

The second group of studies concerns relatively long lived (*i.e.* μs lifetimes) excited triplet states of metal complexes using single-crystal techniques. In this work, high-repetition-rate lasers were used as described above and, as in conventional single-crystal experiments, thousands of reflections were collected. A description of the results follows.

4.1. Picosecond powder diffraction studies of reversible molecular deformation on excitation (A)

The excited states of 4-(dimethylamino)benzonitrile (DMABN) and other substituted aminobenzonitriles have been the subject of extensive discussions since the initial discovery in 1959 of intramolecular charge transfer (ICT) upon photoexcitation in polar solvents, which results in a red-shifted ($\lambda > 400$ nm) ns timescale fluorescence (Lippert *et al.*, 1961, 1962). In polar solvents, fluorescence from both a locally excited (LE) state and the ICT state is observed. For the latter, either a planar intramolecular charge transfer (PICT) state or a twisted state (TICT) with perpendicular arrangement of the amino and phenyl groups have been proposed, based mainly on spectroscopic information, including time-resolved Raman and infrared results. The TR diffraction data represent a direct measurement of the geometry change, which may however be affected by restrictions imposed by the crystal matrix. The room-temperature experiments (Techert *et al.*, 2001; Techert & Zachariasen, 2004) were conducted at the ID-09-TR beamline at ESRF, with a tripled Ti:sapphire laser (λ = 267 nm) operating at a frequency of 897 Hz and monochromatic radiation from an Si(111) monochromator.

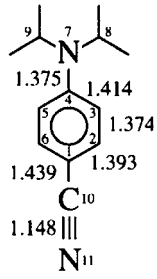

For DMABN (Techert *et al.*, 2001), intensity changes of 1–10% were observed on a timescale of hundredths of picoseconds (Fig. 8). The refinement included rigid-body translations and rotations and the inversion and torsional modes of the substituted amino group of the excited molecule, the excited-state population and unit-cell parameters, while keeping the ground-state geometry constant. The excited-state occupancy was found to vary between 26 and 30% in the first 470 ps after exposure and diminished subsequently. A reduction of the inversion angle defining the non-planarity of the bonds around the N atom from 13 (1) to 3 (1)° and an increase in the torsional angle from 0 (1) to 10 (1)° were reported. The crystal spectrum of DMABN suggests that mainly the LE state is populated on excitation. This is not the case for (4-diisopropylamino)benzonitrile (DIABN), for which the observed intensity changes range from 1 to 8% and excited-state populations are in the 4–5% range during the first ~2000 ps

after excitation (Techert & Zachariasen, 2004). In DIABN, the molecule is not completely planar in the ground state. The twist angle of 14° reduces to an average of 10° for the two independent molecules in the unit cell. The final excited-state geometry is much closer to the 0° PICT than to the 90° TICT structure. At least for the ICT state of DIABN in the crystal, the geometry remains almost planar on excitation.

4.2. Microsecond-resolution studies of the geometry of excited triplet states (B)

4.2.1. The diplatinum tetrapyrophosphite ion. The $[Pt_2(pop)_4]^{4-}$ ion [pop = pyrophosphite, $(H_2P_2O_5)^{2-}$] has an excited $^3A_{2u}$ triplet state which is split by about 42 cm^{-1} into two thermally equilibrated levels because of spin–orbit coupling. As the lower state has a longer lifetime and the upper state becomes much less populated for $kT << 42$ cm^{-1}, the overall lifetime increases rapidly below about 50 K. The first experiments at 17 K were conducted at the X3 beamline at the National Synchrotron Light Source at Brookhaven National Laboratory on $(TEA)_3H[Pt_2(pop)_4]$ (TEA = tetraethylammonium) using 355 nm excitation from an Nd:YAG laser (Kim *et al.*, 2002). In accordance with the expected promotion of a Pt–Pt antibonding $5d\ \sigma^*$ electron to a weakly bonding $6p\ \sigma$ orbital, and with a Franck–Condon analysis of the vibrational fine structure of the spectra (Rice & Gray, 1983; Stiegman *et al.*, 1987), the Pt–Pt bond was found to be shortened on excitation. The experimental shortening of 0.28 (9) Å is accompanied by a 3° rotation of the Pt–Pt axis (Fig. 9). Though the shortening is just at the limit of significance in this first experiment, the value obtained is supported by two subsequent studies. Ozawa and co-workers at the SPring-8 synchrotron source used a multi-exposure imaging-plate technique, in which, for each oscillation range, the imaging plate is slightly shifted after light-off data collection to collect light-on data on the same plate (Ozawa *et al.*, 2003). Their reported shrinkage of the Pt–Pt distance of 0.23 (4) Å in $(TBA)_2H_2(Ptpop)$ (TBA = *n*-tetrabutylammonium) is in good agreement with the first study.

More recently, the shortening has been measured in a mixed salt of the $[Pt_2(pop)_4]^{4-}$ ion with the electron acceptor MV^{2+} (methylviologen, Fig. 10*a*) and K^+ (Gerlits *et al.*, 2004; Gerlits, 2004). The highly reactive excited triplet state of the anion easily transfers an electron to the MV^{2+} cation, leading to a partial quenching of the phosphorescence in $MVK_2[Pt_2(pop)_4]$, and total quenching in crystals of a second salt $(MV)_2[Pt_2(pop)_4]$ without the K atoms. The monoclinic crystals of the mixed salt contain two independent molecules, each located on a center of symmetry, leading to two independent Pt—Pt distances. The Pt—Pt shortenings on excitation are found to be 0.23 (4) and 0.28 (5) Å, with an excited-state population of 6%, rather than the 2 and 1.4% achieved in the first two studies.

Though the excited-state populations are fairly small in all three experiments, the good agreement between the different studies is satisfying and gives confidence in the methods that have been developed.

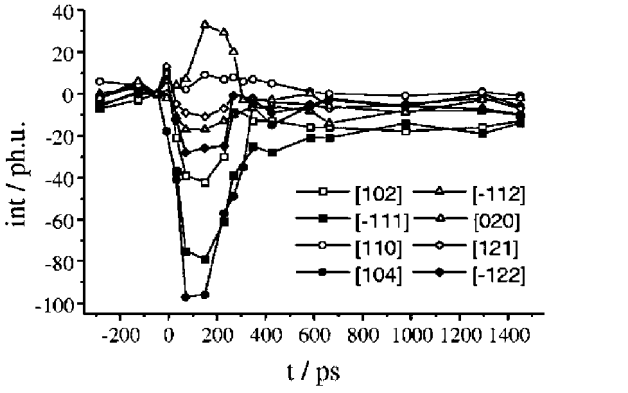

Figure 8
Change of the integrated intensities of a powder diffraction pattern of DMABN after excitation. Intensity changes range from 1 to 10% of the total signal. Reprinted figure with permission from Techert, Schotte & Wulff (2001). *Phys. Rev. Lett.* **86**, 2030–2033. Copyright (2001) by the American Physical Society.

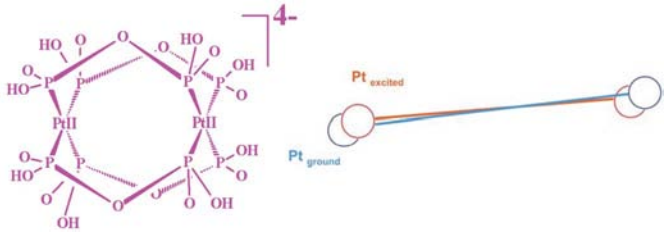

Figure 9
The $[Pt_2(pop)_4]^{4-}$ ion [pop = pyrophosphate, $(H_2P_2O_5)^{2-}$] and the Pt—Pt change on excitation.

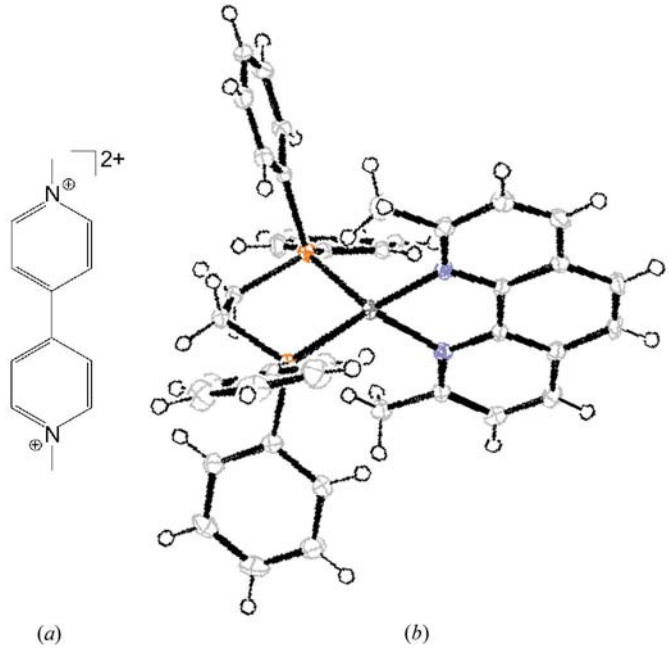

Figure 10
The dimethylviologen (MV) cation and $[Cu^I(dmp)(dppe)]^+$.

4.2.2. Geometry changes of a Cu^{I} phenanthroline complex on photoexcitation in a confining medium by time-resolved X-ray diffraction. Cu^{I} diimine coordination complexes undergo metal-to-ligand or ligand-to-ligand charge transfer upon excitation, leading to relatively long lifetime excited triplet states (Rader *et al.*, 1981; Scaltrito *et al.*, 2000) and a significant distortion relative to the ground-state geometry. The excited state is expected to flatten on transfer of electron density from the metal to the ligands (MLCT), since Cu^{II} favors a planar coordination, while Cu^{I} prefers a tetrahedral geometry. The flattening is much reduced, and the lifetime increased, by 2,9 substitution of the phenanthroline rings (Fig. 10*b*), which sterically prevents large flattening occurring and leads to longer-lifetime excited states.

The highly luminescent excited states have powerful reducing properties. When the molecules are attached by chemisorption to a semiconductor surface and subsequently photo-excited, they can inject electrons into the semiconductor conduction bands and thus form the basis for photovoltaic cells (Hagfeldt & Grätzel, 2000). Cu^{I} diimines and related species are therefore extensively investigated because of their potential for solar energy capture (Scaltrito *et al.*, 2000; Armaroli, 2001).

Replacement of one of the two diimine ligands by a bulky phosphine ligand can lead to complexes with quite long lifetimes. Crystals of Cu^{I}(dmp)(dppe)PF_6 [dmp = 2,9 dimethylphenanthroline, dppe = 1,2-bis(diphenylphosphino)ethane] show a bi-exponential decay of the phosphorescence emission with lifetimes of 88 and 552 µs at 16 K, although the emission of the complex in solution is mono-exponential (Gembicky *et al.*, 2004). The compound crystallizes in the monoclinic space group $P2_1/c$ with two independent molecules in the asymmetric unit. The time-resolved analysis (Coppens, Vorontsov *et al.*, 2004) was based on 9154 independent response ratios with $\eta > 2\sigma(\eta)$ from three data sets. The distortion of one of the two molecules is depicted in Fig. 11. The second molecule is already slightly flattened in the ground state and does not undergo a further change in this distortion. It is of interest that the two independent molecules distort differently on excitation and are found to have different excited-state populations on exposure. This finding, combined with the bi-exponential decay in the crystal, but not in solution, suggests that the lifetimes of the two independent molecules in the crystals differ, which is plausible as energy transfer to the environment, which corresponds to luminescence quenching, is a function of the interaction with the molecule's neighbors. It is also in agreement with the energy gap law, according to which a smaller excited-state distortion corresponds to a longer lifetime of the excited state (Freed & Jortner, 1970; Turro, 1978; Scaltrito *et al.*, 2000). There are no other techniques that can provide such site-specific information on photophysical behavior of molecules in crystals.

4.2.3. A very large contraction on excitation of a d^8–d^8 dirhodium complex. As pointed out by Miskowski *et al.* (1994), the ground-state Rh—Rh bond length in $[Rh_2(dimen)_4]^{2+}$ (dimen = 1, 8-diisocyanomenthane) (Fig. 12) salts shows an unusually large variation, the distance being equal to 4.48 Å in the PF_6^- and 3.861 Å in the $[B(C_6H_5)_4]_2$ salts. In agreement with the softness of this distance, analysis of the band shape of the absorption spectra of $[Rh_2(diprop)_4]^{2+}$ (diprop = 1, 3-diisocyanopropane) reveals a significant contraction of ~0.3 Å upon excitation to the ^3A_u excited state (Rice & Gray, 1981). This result is supported by later density functional theory (DFT) calculations, which for the ground state give a contraction of 0.39 Å on excitation, corresponding to a $4d\ \sigma^* \rightarrow 5p\ \sigma$ excitation of the d^8–d^8 complex (Novozhilova *et al.*, 2004).

In the TR experiment on the $[Rh_2(dimen)_4]PF_6$ salt (Coppens, Gerlits *et al.*, 2004), 6717 response ratios larger than $2\sigma(\eta)$ were measured at a nominal temperature of 17 K. The final excited-state Rh—Rh distance is found to be 3.64 (5) Å, compared with the ground-state value of 4.5153 (3) Å (90 K) and 4.496 (1) Å at 17 K corresponding to a shortening of 0.86 (5) Å. This represents by far the largest structural change on excitation observed by atomic resolution time-resolved diffraction methods.

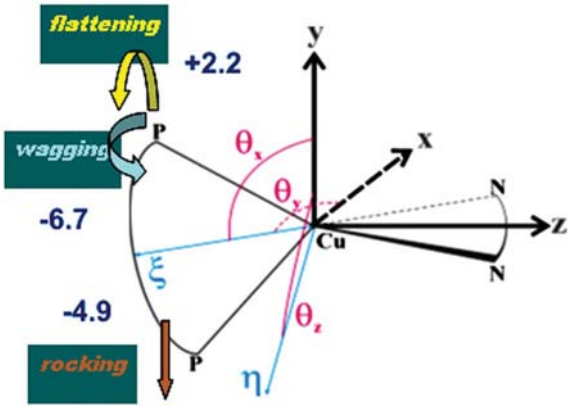

Figure 11
The increase in flattening and decrease in the wagging and rocking distortions of one of the $[Cu^{I}(dmp)(dppe)]^{+}$ ions in the crystal on excitation.

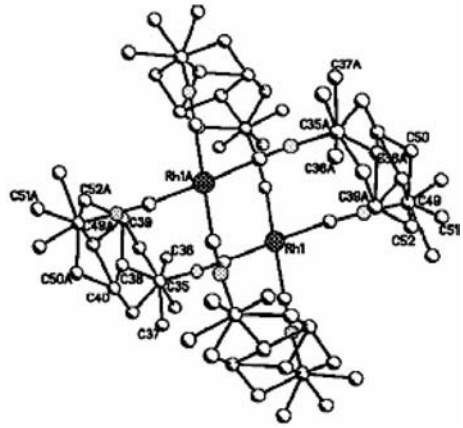

Figure 12
Drawing of the $[Rh_2(dimen)_4]^{2+}$ ion in the crystal. Note the disorder in the bridging ligands.

In addition to the bond shortening, a rotation of 13 (1)° of the molecule on excitation in the crystal is observed. Excited-state populations refined to 1.9% (532 nm excitation) and 2.5% (355 nm) in the two crystals, respectively. Because of the small populations achieved, no experimental information on the shift of the lighter atoms could be obtained, although parallel DFT calculations of the excited state give some insight into the ligand deformations. As expected, the isocyano groups are tilted to follow the Rh—Rh contraction, but the distortions in the stiff dimenthane ligand appear minor.

5. Comparison of theoretical and TR diffraction results for excited-state geometry

DFT calculations have been exceedingly successful in the calculation of ground-state properties, but the theorems on which they are based are strictly valid only for the ground-state wavefunction (Hohenberg & Kohn, 1964; Kohn & Sham, 1965). The importance of the development of techniques for the calculation of excited-state geometry has been emphasized, as excited-state experimental data are more difficult to obtain and interpret than ground-state data (Rappoport & Furche, 2004). Recent developments of linear response theory applied in TD-DFT (time-dependent DFT) have now allowed successful calculation of not only the energy but also the geometry of a number of excited-state geometries (Furche & Ahlrichs, 2002), including those of two of the singlet excited states of DMABN (Rappoport & Furche, 2004), which has also been calculated with *ab initio* CI (configuration interaction) methods (Menucci *et al.*, 2000). For DMABN, both methods agree that the ICT (intermolecular charge transfer) structure has a 90° twisted geometry, though the originally proposed TICT and PICT models are found to be much too oversimplified to give a good representation of the excited-state electronic structure. The theoretical conclusion does not agree with the experimental TR powder results on DIABN and raises the question of the constraining influence of the crystal matrix on the photochemical behavior in the solid state.

For more complex molecules, the required parallel processing has not yet been incorporated in the available computer codes for TD-DFT geometry optimization of the excited states, and other methods must be used. Spin-unrestricted DFT calculations on the ms-lifetime triplet states of the lowest energy have been performed with the Amsterdam Density Functional (ADF) program (Theoretical Chemistry, Vrije Universiteit, Amsterdam, The Netherlands, http://www.scm.com; Fonseca Guerra *et al.*, 1998; te Velde *et al.*, 2001). For the $[Pt_2(pop)_4]^{4-}$ ion, calculations with different functionals employing quasirelativistic Pauli and ZORA (zeroth-order regular approximate relativistic equation) formalisms all predict a Pt—Pt bond shortening and a slight Pt—P lengthening upon excitation to the lowest triplet state, as summarized in Fig. 13. The PW86LYP functional with the ZORA relativistic treatment is found to produce good agreement with both TR-crystallographic and spectroscopic results. Calculation of the spin density shows it to be mainly localized on the Pt atoms, in accordance with the ability of the triplet excited state to abstract H and halogen atoms from organic substrates.

For $[Cu^{I}(dmp)(dmpe)]^{+}$ [dmpe = 1,2-bis(dimethylphosphino)ethane], which is used as a reference ion for the dppe complex, the calculated flattening is, at 8°, much larger than the observed flattening of 3.2° and less in the two independent molecules, whereas the computed reduction in the rocking and wagging distortions are closer to the observed values. According to the calculations, the electron transfer on excitation is mostly ligand to ligand, dimethylphenanthroline being the acceptor, while the Cu-atom charge changes by only ~+0.1 e, which is close to the difference between the corresponding Cu^{II} and Cu^{I} complexes.

Theoretical results on $[Rh_2(dimen)_4]^{2+}$ (ZORA relativistic approach, VWNBLYP density functional, Slater-type triple-ζ basis set for Rh, double-ζ with polarization function basis set for the other atoms) show a shallow potential-energy minimum and an Rh–Rh distance of 4.647 Å shortening to 3.107 Å on excitation. This corresponds to an increase in Mayer bond order (Mayer, 1983, 1984) from 0.019 to 0.863, as calculated with the program of Bridgeman and Empson (Bridgeman *et al.*, 2001; Bridgeman & Empson, 2003). Thus, the contraction calculated theoretically is significantly larger than actually observed in the crystal. In a sense, this is similar to the reduced distortion observed for $[Cu^{I}(dmp)(dppe)]PF_6$ and for DMABN, but in the latter cases a considerable change in the shape of the molecule occurs, while a contraction as occurs for Rh—Rh should be less impeded by the molecular environment. Nevertheless, the overall picture that is emerging from the studies now available is one of a considerable

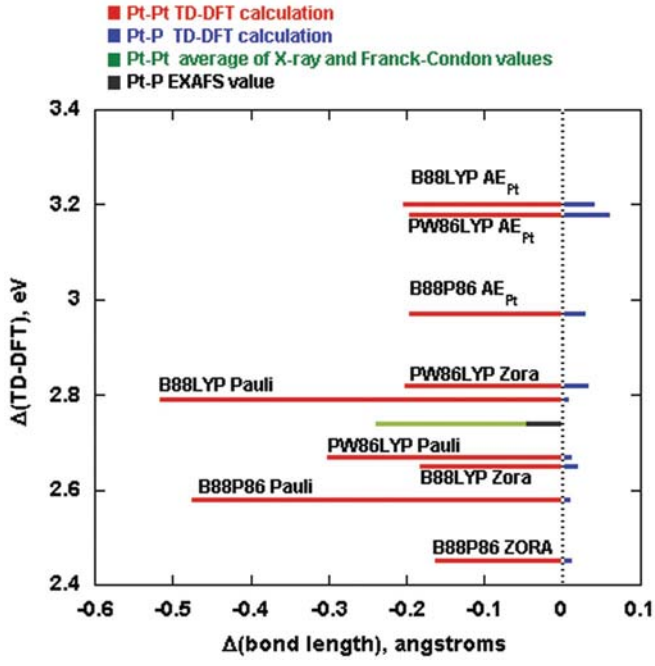

Figure 13
Pt—Pt (red) and Pt—P (blue) bond changes *versus* TD-DFT lowest singlet-triplet excitation energy and comparison with the experimental values (green and grey for Pt—Pt and Pt—P changes, respectively). From Novozhilova *et al.* (2003).

reduction of the geometry distortion on excitation in the solid state and a strong effect of the crystal matrix on photophysical behavior.

6. Concluding remarks

It is clear from the small number of studies at atomic resolution that have been completed that the field is still in its infancy. Progress may be expected by further development of pink beam techniques, coupled with high-repeat-rate lasers with narrower pulse widths. The ultimate goal of the monitoring of chemical processes in crystals at the atomic level seems technically well within reach. It is clear that we are at the beginning of a new era in dynamic X-ray diffraction research in which our insight into the atomic mechanism of a broad range of dynamic processes will be significantly enhanced.

Time-resolved experiments at the ID-15 beamline made possible through support from DOE grant DE-FG02-02ER15372. Methods development and interpretation funded by the National Science Foundation through grant CHE0236317. Theoretical calculations were performed at the Center for Computational Research of the University at Buffalo. The 15-ID beamline is funded through NSF CHE0087817. Use of the Advanced Photon Source was supported by the US Department of Energy, Office of Basic Energy Sciences, under contract No. W-31-109-ENG-38.

References

Anderson, S., Srajer, V., Pahl, R., Rajagopal, R., Schotte, F., Anfinrud, P., Wulff, M. & Moffat, K. (2004). *Structure*, **12**, 1039–1045.
Armaroli, N. (2001). *Chem. Soc. Rev.* **30**, 113–124.
Bourgeois, D., Wagner, U. & Wulff, M. (2000). *Acta Cryst.* D**56**, 973–985.
Bridgeman, A. J., Cavigliasso, G., Ireland, L. R. & Rothery, J. (2001). *J. Chem. Soc. Dalton Trans.* pp. 2095–2108.
Bridgeman, A. J. & Empson, C. J. (2003). The University of Hull, England.
Carducci, M. D., Pressprich, M. R. & Coppens, P. (1997). *J. Am. Chem. Soc.* **119**, 2669–2678.
Collet, E., Lemée-Cailleau, M.-H., Buron-Le Cointe, M., Cailleau, H., Wulff, M., Luty, T., Koshihara, S.-Y., Meyer, M., Toupet, L., Rabiller, P. & Techert, S. (2003). *Science*, **300**, 612–615.
Coppens, P. (1992). *Synchrotron Radiation Crystallography*. London: Academic Press.
Coppens, P., Fomitchev, D. V., Carducci, M. D. & Culp, K. (1998). *J. Chem. Soc. Dalton Trans.* pp., 865–872.
Coppens, P., Gerlits, O., Vorontsov, I. I., Kovalevsky, A. Y., Chen, Y.-S., Graber, T. & Novozhilova, I. V. (2004). *Chem. Commun.* pp. 2144–2145.
Coppens, P., Novozhilova, I. & Kovalevsky, A. Yu. (2002). *Chem. Rev.* **102**, 861–884.
Coppens, P., Vorontsov, I. I., Graber, T., Kovalevsky, A. Yu., Chen, Y.-S., Wu, G., Gembicky, M. & Novozhilova, I. V. (2004). *J. Am. Chem. Soc.* **126**, 5980–5981.
Enkelmann, V., Wegner, G., Novak, K. & Wagener, K. B. (1993). *J. Am. Chem. Soc.* **115**, 10390–10391.
Fonseca Guerra, C., Snijders, J. G., te Velde, G. & Baerends, E. J. (1998). *Theor. Chem. Acc.* **99**, 391–403.
Freed, K. F. & Jortner, J. (1970). *J. Chem Phys.* **52**, 6272–6291.
Fullagar, W. K., Wu, G., Kim, C., Ribaud, L., Sagerman, G. & Coppens, P. (2000). *J. Synchrotron Rad.* **7**, 229–235.
Furche, F. & Ahlrichs, R. (2002). *J. Chem. Phys.* **117**, 7433–7447.
Gembicky, M., Kovalevsky, A., Page, P. M., Bright, F. V. & Coppens, P. (2004). Unpublished data.
Gerlits, O. (2004). Thesis, State University of New York at Buffalo, USA.
Gerlits, O., Kovalevsky, A. Yu. & Coppens, P. (2004). Abstracts 228th Am. Chem. Soc. National Meeting, 22–26 August 2004.
Guérin, L., Collet, E., Lemee-Cailleau, M.-H., Buron-Le Cointe, M., Cailleau, H., Plech, A., Wulff, M., Koshihara, S.-Y. & Luty, T. (2004). *Chem. Phys.* **299**, 163–170.
Hagfeldt, A. & Grätzel, M. (2000). *Acc. Chem. Res.* **33**, 269–277.
Headrick, R. L., Smolenski, K. W., Kazimirov, A., Liu, C. & Macrander, A. T. (2002). *Rev. Sci. Instrum.* **73**, 1476–1479.
Hohenberg, P. & Kohn, W (1964). *Phys. Rev.* **136**, 864–871.
Kim, C. D., Pillet, S., Wu, G., Fullagar, W. K. & Coppens, P. (2002). *Acta Cryst.* A**58**, 133–137.
Kohn, W. & Sham, L. J. (1965) *Phys. Rev.* **140**, A1133–A1138.
Kovalevsky, A. Yu., Bagley, K. A., Cole, J. M. & Coppens, P. (2003). *Inorg. Chem.* **42**, 140–147.
Kovalevsky, A. Yu., Bagley, K. A. & Coppens, P. (2002). *J. Am. Chem. Soc.* **124**, 9241–9248.
Krueger, A. & Féru, P. (2004) *Photonics Spectra*, March issue. Available upon request from http://www.photonics.com/spectra/features/XQ/ASP/artabid.751/QX/read.htm.
LeGrand, A. D., Schildkamp, W. & Blank, B. (1989). *Nucl. Instrum. Methods*, A**275**, 442–446.
Lippert, E., Lüder, W. & Boos, H. (1962). *Advances in Molecular Spectroscopy*. European Conference on Molecular Spectroscopy, Bologna, Italy, 1959, edited by A. Mangini, p. 443. Oxford: Pergamon Press.
Lippert, E., Lüder, W., Moll, F., Nägele, W., Boos, H., Prigge, H. & Seibold-Blankenstein, I. (1961). *Angew. Chem.* **73**, 695–706.
McPherson, A., Wang, J., Lee, P. L. & Mills, D. M. (2000). *J. Synchrotron Rad.* **7**, 1–4.
Martynov, V. V., Platonov, Y., Kazimirov, A. & Bilderback, D. H. (2003). *Proc. SPIE*, **5195**, 46–53.
Mayer, I. (1983). *Chem. Phys. Lett.* **97**, 270–274.
Mayer, I. (1984). *Int. J. Quantum Chem.* **26**, 151–154.
Miskowski, V. M., Rice, S. F., Gray, H. B., Dallinger, R. F., Milder, S. J., Hill, M. J., Exstrom, C. L. & Mann, K. R. (1994). *Inorg. Chem.* **33**, 2799–2807.
Menucci, B., Toniolo, A. & Tomasi, J. (2000). *J. Am. Chem. Soc.* **122**, 10621–10630.
Moffat, K. (2001). *Chem. Rev.* **101**, 1569–1581.
Novozhilova, I., Volkov, A. V. & Coppens, P. (2003). *J. Am. Chem. Soc.* **125**, 1079–1087.
Novozhilova, I. V., Volkov, A. V. & Coppens, P. (2004). *Inorg. Chem.* **43**, 2299–2307.
Ozawa, Y., Pressprich, M. R. & Coppens, P. (1998). *J. Appl. Cryst.* **31**, 128–135.
Ozawa, Y., Terashima, M., Mitsumi, M., Toriumi, K., Yasuda, N., Uekusa, H. & Ohashi, Y. (2003). *Chem. Lett.* **32**, 62–63.
Rader, R. A., McMillin, D. R., Bucker, M. T., Matthews, T. G., Gasadonte, D. J., Lengel, R. K., Whittaker, S. B., Darmon, L. M. & Lytle, F. E. (1981). *J. Am. Chem. Soc.* **103**, 5906–5912.
Rajagopal, S., Schmidt, M., Anderson, S., Ihee, H. & Moffat, K. (2004). *Acta Cryst.* D**60**, 860–871.
Rappoport, D. & Furche, F. (2004). *J. Am. Chem. Soc.* **126**, 1277–1284.
Reeuwijk, S. J. van, Puig-Molina, A. & Graafsma, H. (2000). *Phys. Rev. B*, **62**, 6192–6197.
Ren, Z., Perman, B., Srajer, V., Teng, T.-Y., Pradervand, C., Bourgeois, D., Schotte, F., Ursby, T., Kort, O. R., Wulff, M. & Moffat, K. (2001). *Biochemistry*, **40**, 13788–13801.
Rice, S. F. & Gray, H. B. (1981). *J. Am. Chem. Soc.* **103**, 1593–1595.

Rice, S. F. & Gray, H. B. (1983). *J. Am. Chem. Soc.* **105**, 4571–4575.
Rodriguez, J. A., Hanson, J. C., Frenkel, A. I., Kim, J.-Y. & Perez, M. J. (2002). *J. Am. Chem. Soc.* **124**, 346–354.
Scaltrito, D. V., Thompson, D. W., O'Callaghan, J. A. & Meyer, G. J. (2000). *Coord. Chem. Rev.* **208**, 243–266.
Schotte, F., Anfinrud, P. A. & Wulff, M. (2002). *Trends Optics Photonics*, **72**, 31–32.
Schotte, F., Lim, M., Jackson, T. A., Smirnov, A. V., Soman, J., Olson, J. S., Phillips, G. N. Jr, Wulff, M. & Anfinrud, P. A. (2003). *Science*, **300**, 1944–1947.
Srajer, V., Ren, Z., Teng, T.-Y., Schmidt, M., Ursby, T., Bourgeois, D., Pradervand, C., Schildkamp, W., Wulff, M. & Moffat, K. (2001). *Biochemistry*, **40**, 13802–13815.
Stiegman, A. E., Rice, S. F., Gray, H. B. & Miskowski, V. M. (1987). *Inorg. Chem.* **26**, 1112–1116.
Techert, S., Schotte, F. & Wulff, M. (2001). *Phys. Rev. Lett.* **86**, 2030–2033.
Techert, S. & Zachariasen, K. A. (2004). *J. Am. Chem. Soc.* **126**, 5593–5600.
Turro, N. J. (1978). *Modern Molecular Photochemistry*. Sausalito, CA: University Science Books.
Velde, G. te, Bickelhaupt, F. M., van Gisbergen, S. J. A., Fonseca Guerra, C., Baerends, E. J., Snijders, J. G. & Ziegler, T. (2001). *J. Comput. Chem.* **22**, 931–967.
Vorontsov, I. I. & Coppens, P. (2005). To be submitted.
Wong, J., Larson, E. M., Holt, J. B., Waide, P. A., Rupp, B. & Frahm, R. (1990). *Science*, **249**, 1406–1409.
Wulff, M., Plech, A., Eybert, L., Schotte, F. & Afinrud, P. (2003). *Faraday Discuss.* **122**, 13–26.
Ziegler, E., Hignette, O., Morawe, C. & Tucoulou, R. (2001). *Nucl. Instrum. Methods Phys. Res.* A**467–468**, 954–957.